ACS OMEGA

http://pubs.acs.org/journal/acsodf

Article

Alternative Causal Link between Peptide Fibrillization and β-Strand Conformation

Zhihua Xing, Yongzhu Chen, and Feng Qiu*

Cite This: *ACS Omega* 2021, 6, 12904−12912

Read Online

ACCESS | Metrics & More | Article Recommendations | Supporting Information

ABSTRACT: In the prevailing phenomenon of peptide fibrillization, β-strand conformation has long been believed to be an important structural basis for peptide assembly. According to a widely accepted theory, in most peptide fibrillization processes, peptide monomers need to intrinsically take or transform to β-strand conformation before they can undergo ordered packing to form nanofibers. In this study, we reported our findings on an alternative peptide fibrillization pathway starting from a disordered secondary structure, which could then transform to β-strand after fibrillization. By using circular dichroism, thioflavin-T binding test, and transmission electron microscopy, we studied the secondary structure and assembly behavior of Ac-RADARADARADARADA-NH_2 (RADA16-I) in a low concentration range. The effects of peptide concentration, solvent polarity, pH, and temperature were investigated in detail. Our results showed that at very low concentrations, even though the peptide was in a disordered secondary structure, it could still form nanofibers through intermolecular assembly, and under higher peptide concentrations, the transformation from the disordered structure to β-strand could happen with the growth of nanofibers. Our results indicated that even without ordered β-strand conformation, driving forces such as hydrophobic interaction and electrostatic interaction could still play a determinative role in the self-assembly of peptides. At least in some cases, the formation of β-strand might be the consequence rather than the cause of peptide fibrillization.

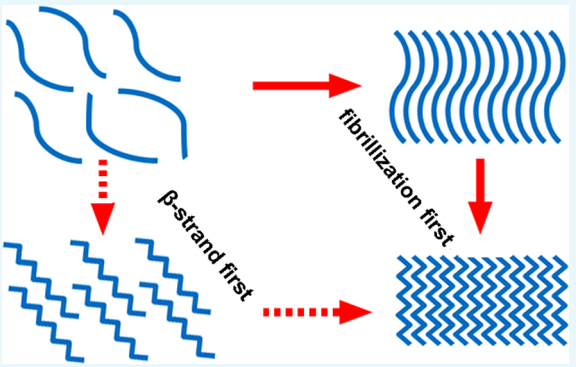

INTRODUCTION

As an important category of nanobiomaterials, nanofibers formed by designer self-assembling peptides (SAPs) have been extensively investigated for many years.[1−3] Due to their similarity to pathogenic amyloid fibrils formed by natural peptides or proteins, these nanofibers have also been ideal models for studying the mechanism of amyloid-like fibrillization.[4,5] In the past two decades, numerous studies have shown that most SAP nanofibers were composed of β-sheet units, which were the parallel or antiparallel alignment of peptide chains in β-strand conformation.[6−8] This led to the general belief that β-strand conformation of individual peptide monomers was pivotal for supporting peptide fibrillization. For this reason, peptide fragments taking β-strand conformation have also been regarded as the essential motif for self-assembly in many SAP systems.[9−11]

However, in recent years, more and more studies have indicated that the importance of a highly ordered β-sheet for the formation of SAP nanofibers is not so incontrovertible. Tripeptides that could form nanofibers based on disordered conformation have been reported recently.[12,13] Worm-like micelles, very short nanofibers, or even long thin nanofibers were also formed by peptides taking random coil conformation.[14,15] Our group has also designed many amphiphilic peptides that could self-assemble into nanofibers with the absence of the β-sheet.[16−18] On the other hand, computational studies have suggested that in the early stage of self-assembly, some peptide amphiphiles mainly took a random coil secondary structure.[19,20] All these studies suggested the possibility of peptide fibrillization based on non-β-strand conformation, challenging the traditional fibrillization theory based on β-strand.

Considering these controversial findings about secondary structure supporting peptide fibrillization, a more easily accepted theory has risen that non-β-strand peptides could undergo fibrillization, accompanying which the conformation of peptide monomers also transformed to β-strand.[21−25] Following the textbook theory that the secondary structure determines the tertiary structure, it seems to be reasonable to presume that disordered peptide monomers should transform to β-strand conformation before they can self-assemble into nanofibers. However, for these intrinsically disordered

Received: March 16, 2021
Accepted: April 23, 2021
Published: May 5, 2021

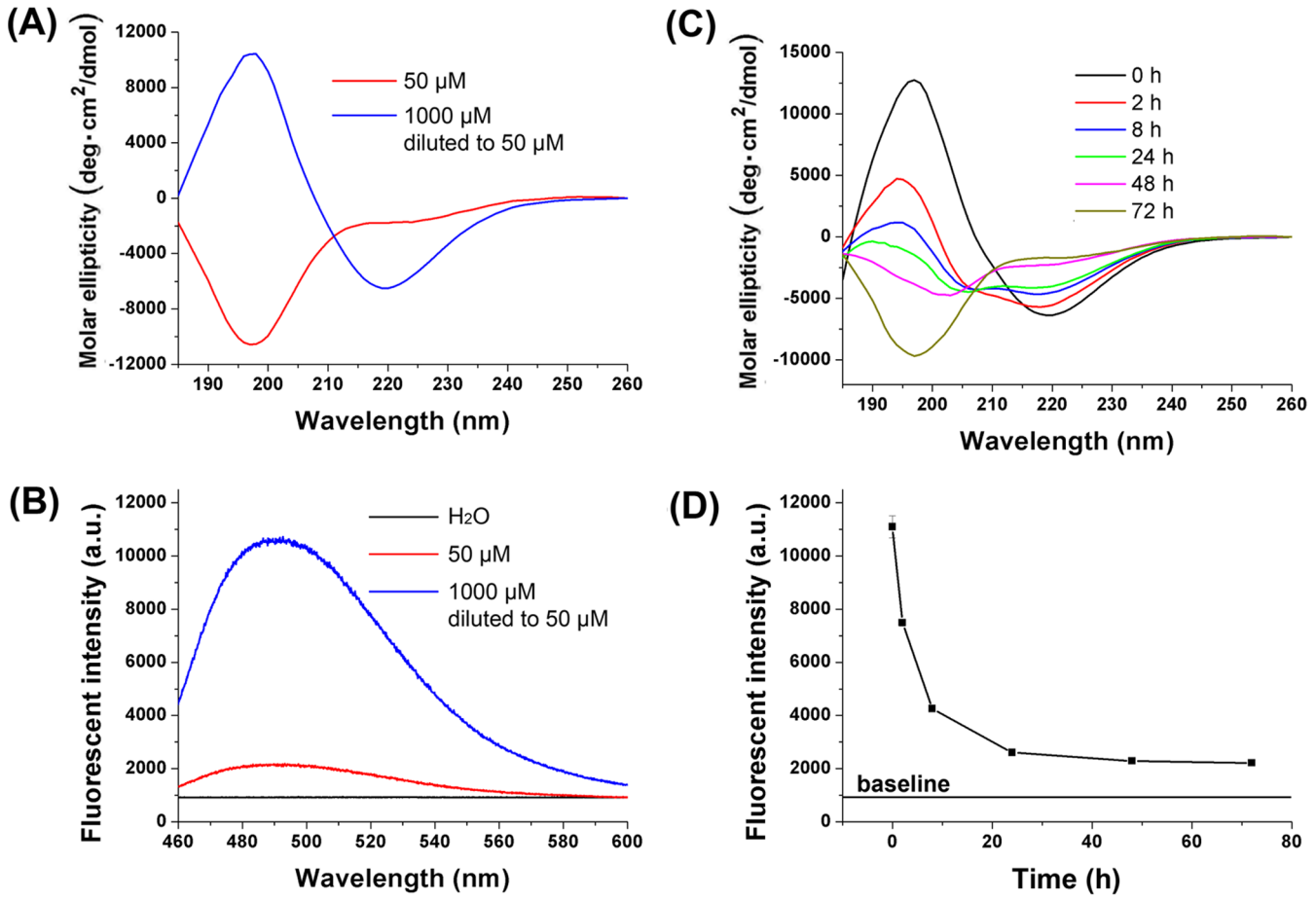

Figure 1. Secondary structure and fibrillization state of RADA16-I determined by peptide concentration. (A) CD spectrum of the original 50 μM sample showed a signal of disordered conformation, while the 50 μM sample diluted from the 1000 μM solution showed a β-strand signal. (B) Thioflavin-T (ThT)-binding fluorescence showed that the 50 μM sample diluted from the 1000 μM solution had a much higher fibrillization signal. In both (A) and (B), the signal for the diluted sample was measured immediately after dilution. (C) Change in the CD signal after dilution from 1000 to 50 μM. (D) Change in ThT-binding fluorescence after dilution from 1000 to 50 μM.

peptides, very few research studies have been systematically carried out to clarify the causal link between peptide fibrillization and β-strand conformation, i.e., which one comes first.

In fact, some experimental findings seemed to be on the opposite of this presumption. As one of the most widely investigated SAP motifs, Ac-RADARADARADARADA-NH_2 (RADA16-I) has been substantially proved to take typical β-strand conformation at a higher concentration of 0.5−2% (w/v, approximately equal to 3−12 mM), which was thought to be its structural basis for fibrillization.[26−29] However, a recent study showed that at a lower concentration of 0.1 mM, some peptides based on the RADA16-I motif took random coil conformation instead of β-strand, while they could still form typical nanofibers at even lower concentrations.[30] Similar concentration-dependent paradox on peptide conformation has also been found in amphiphilic peptides such as DAAAAAAD (DA6D), which showed the characteristic feature of the β-sheet in its concentrated dry film, while nanofibers could be formed in diluted solution based on disordered conformation.[18] These findings suggested that although β-strand conformation is strongly linked with peptide fibrillization, it may not necessarily be the starting conformation triggering the fibrillization process.

Taking all these previous findings into consideration, the causal link between peptide fibrillization and β-strand conformation is worth a reevaluation. For this purpose, in this study, we focused on the self-assembling behavior of RADA16-I in a very low concentration range. The effects of peptide concentration, solvent polarity, pH value, and heat shock on the secondary structure and fibrillization behavior of the peptides were investigated. Our results indicated an alternative peptide fibrillization pathway starting from disordered conformation, which gradually transformed to β-strand as a result of compact packing in the fibrillization process.

RESULTS AND DISCUSSION

Circular Dichroism (CD) for Measuring the Peptide Secondary Structure at a Low Concentration. As we know, CD is the major method for monitoring the secondary structure of peptides at a low concentration of around 100 μM. On the contrary, other methods such as X-ray diffraction, Fourier transform infrared spectroscopy, and nuclear magnetic resonance usually need highly concentrated solutions or even dried samples.[31] Interestingly, many previous studies reporting the existence of the β-sheet in SAP nanofibers have been based on the latter three methods. Considering the fact that SAPs will aggregate above a certain concentration, these previous

https://doi.org/10.1021/acsomega.1c01423
ACS Omega 2021, 6, 12904−12912

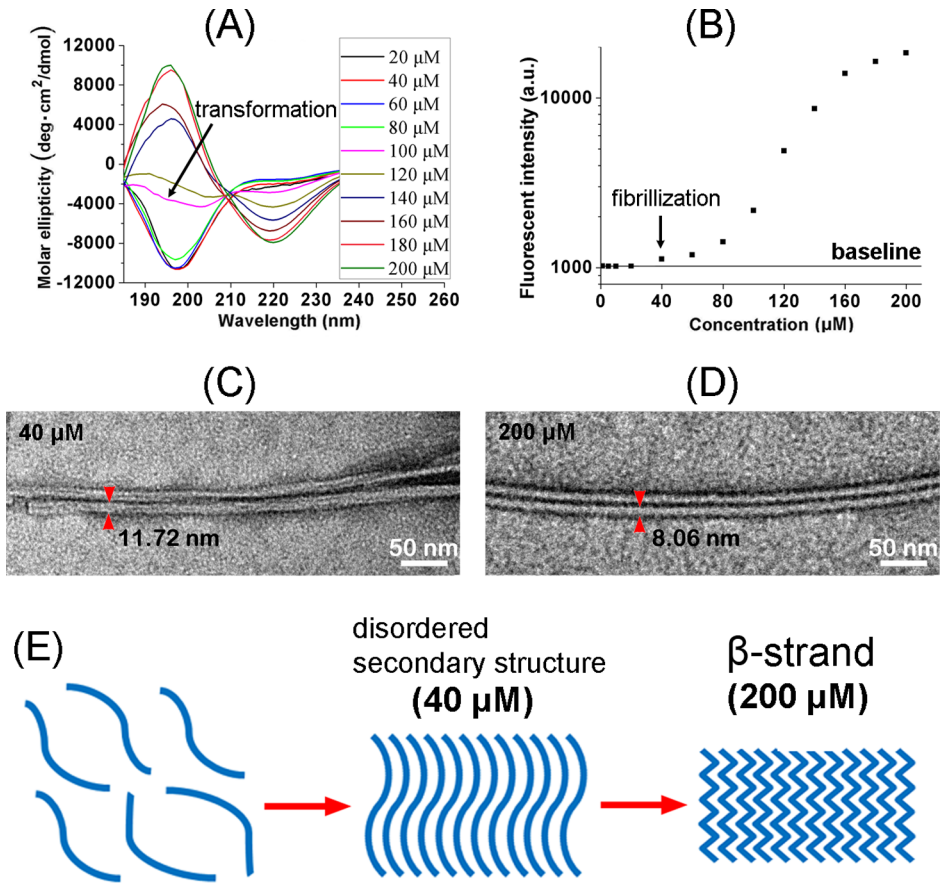

Figure 2. Conformational transition and self-assembly of RADA16-I at different concentrations. (A) CD spectra showed that the conformational transition from the disordered structure to β-strand began at 100 μM. (B) ThT-binding fluorescence showed that self-assembly began at 40 μM. (C) Transmission electron microscopy (TEM) image of nanofibers formed at 40 μM. (D) TEM image of nanofibers formed at 200 μM. (E) Proposed model explaining how the peptide formed nanofibers with different widths based on different secondary structures.

studies were actually inspecting the peptides' secondary structure in their already-assembled state, while their secondary structure at lower concentrations, i.e., around or below their critical aggregation concentration has been neglected. Taking this into consideration, in this study, we used CD to measure the secondary structure of RADA16-I in a very low concentration range.

Concentration Determined the Secondary Structure and Assembling Behavior of RADA16-I. First, RADA16-I was prepared as 50 and 1000 μM samples. The 50 μM sample was directly used for CD measurement, while the 1000 μM sample was diluted to 50 μM just before the CD measurement. Surprisingly, instead of showing a β-strand signal, the original 50 μM sample exhibited a negative peak between 195 and 200 nm, indicating the predominance of disordered conformation. On the contrary, the sample diluted from the 1000 μM solution showed a positive peak between 195 and 200 nm and a negative peak between 215 and 220 nm, which were assigned to typical β-strand conformation (Figure 1A).

In a previous study, we have shown the amyloid-like property of RADA16-I nanofibers, which allowed us to quantitatively analyze the assembling state of the peptide by Thioflavin-T (ThT) -binding fluorescence.[32] As shown in Figure 1B, both samples exhibited a typical fluorescence peak around 495 nm, indicating the formation of amyloid-like nanofibers. However, samples diluted from the 1000 μM solution showed a much higher fluorescent value, indicating a much higher level of assembly.

Although tested at the same concentration of 50 μM, the two samples exhibited quite different secondary structures and fibrillization states. It is quite clear that the sample diluted from the 1000 μM solution was actually exhibiting the secondary structure and the self-assembling state preformed at a higher concentration, which have not been changed immediately after dilution. Interestingly, the secondary structure and the self-assembling state of this sample did change slowly after dilution. As shown in Figure 1C, after diluted from 1000 to 50 μM, the secondary structure of RADA16-I gradually transformed from β-strand to disordered conformation. At the same time, the ThT-binding fluorescence of the peptide also dropped to a stable value within 72 h, suggesting gradual disassembly of the peptide (Figure 1D). However, it should be noted that the stable fluorescence value after 72 h was still far above the baseline, which was coincident with the fact that even at a concentration of 50 μM, the peptide could still self-assemble.

Although it is not surprising that the β-strand conformation of RADA16-I could be destroyed by many factors such as pH and temperature, this is the first time to show that RADA16-I could transform from β-strand to disordered conformation simply by dilution. This result raised the question of what is the intrinsic conformation of the peptide monomer. It is clear that rather than intrinsically taking β-strand conformation as generally believed, RADA16-I could take disordered con-

https://doi.org/10.1021/acsomega.1c01423
ACS Omega 2021, 6, 12904−12912

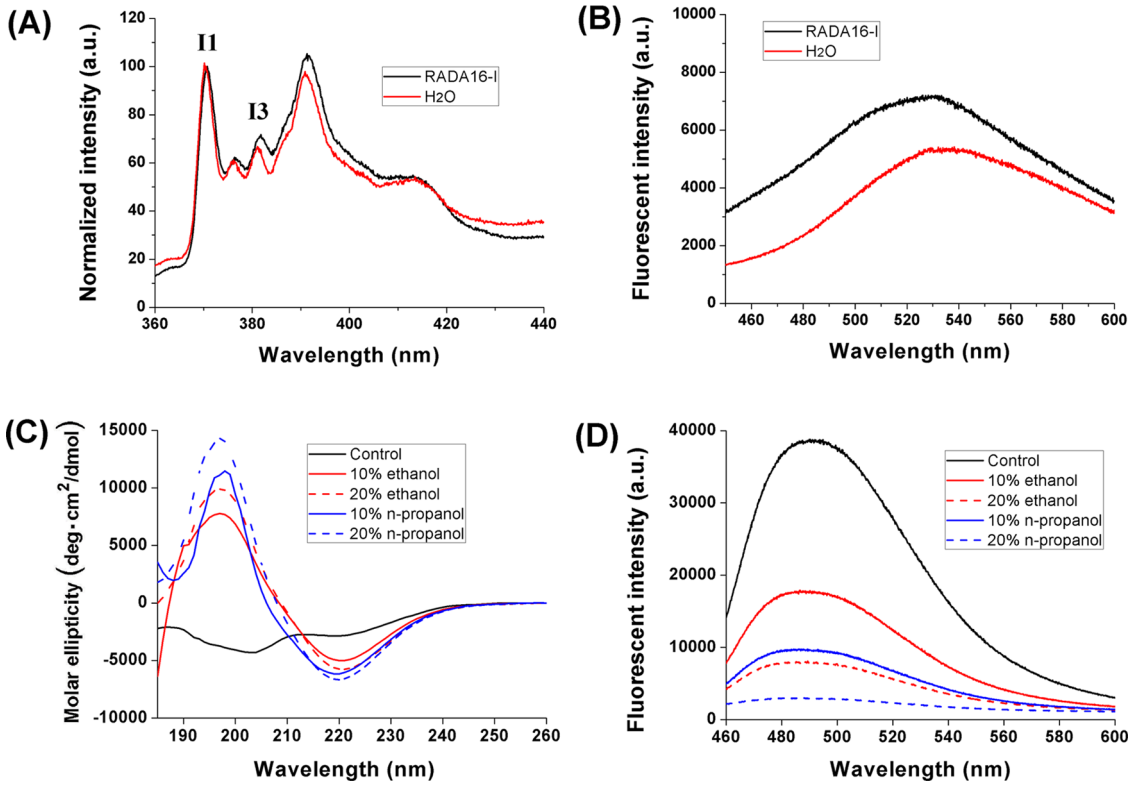

Figure 3. Hydrophobic interaction determined the self-assembling ability of RADA16-I. Both pyrene-binding fluorescence (A) and ANS-binding fluorescence (B) proved the existence of hydrophobic interaction. Changes in the CD spectra (C) and ThT-binding fluorescence (D) of RADA16-I with the presence of organic solvents were exhibited.

formation at a very low concentration, which also seemed capable of supporting the self-assembly of the peptide.

RADA16-I Fibrillization Prior to the Formation of the *β*-sheet. To study how peptide concentration determined the secondary structure and the fibrillization state in detail, RADA16-I samples with concentrations ranging from 1 to 200 μM were prepared. Their secondary structure and fibrillization state were monitored by CD and ThT-binding fluorescence, respectively. As shown in Figure 2A, CD spectra showed that RADA16-I samples at concentrations of 20, 40, and 60 μM were kept in a disordered conformation with a similar CD signal, which gradually transformed to β-strand as the concentration increased. At a concentration of 100 μM, the peptide began to show the obvious β-strand signal. It should be noted that RADA16-I solutions with concentrations of 1, 5, and 10 μM were close to the detectable limitation of the CD measurement so that they were not shown in the results. But according to the trend shown in Figure 2A, it is very unlikely that RADA16-I would take β-strand conformation at these even lower concentrations.

Corresponding to the change in the secondary structure, the ThT-binding fluorescence of RADA16-I also gradually increased with concentration, indicating the growth of amyloid-like nanofibers (Figure 2B). Interestingly, although RADA16-I showed the obvious β-strand signal only at concentrations above 100 μM, its fibrillization began at a much lower concentration of 40 μM, which confirmed that the peptide could form nanofibers based on disordered conformation. Although the ThT-binding fluorescence of the 40 μM sample seemed to be weak, the spectrum in Figure S1 clearly showed its characteristic fluorescence peak. On the other hand, it should be noticed that ThT-binding fluorescence increased more quickly between 80 and 160 μM. This region was approximately overlapped with the concentration range within which the peptide transformed from disordered conformation to β-strand. This result suggested that the formation of β-strand did facilitate the self-assembling process of RADA16-I, probably by packing peptide monomers in a more ordered way.

The formation of supramolecular nanostructures in the 40 and 200 μM samples was further confirmed by dynamic light scattering (DLS). As shown in Figure S2, the size distribution for the 40 μM sample was around 100 nm with a mean *z*-average size of 90.82 $\pm$ 4.95 nm, while the 200 μM sample exhibited a broader size distribution between 30 and 2000 nm with a mean z-average size of 114.77 $\pm$ 2.57 nm. However, it should be noted that DLS as a method for studying particles may not accurately reflect the size of nanofibers with a high aspect ratio. Anyway, these DLS results further confirmed the formation of nanostructures in both samples. Combined with its much stronger ThT-binding fluorescence, the broader size distribution and bigger average size of the 200 μM sample indicated that it formed more or longer nanofibers than the 40 μM sample.

TEM images showed that both 40 and 200 μM samples formed nanofibers, which further confirmed the self-assembling behavior under these concentrations (Figure 2C,D). To confirm the prevalence of these two types of nanofibers, additional TEM images are shown in Figure S3. However, it should be noticed that the width of nanofibers formed by the 40 μM sample was about 11.72 nm, while that of nanofibers formed by the 200 μM sample was about 8.06 nm. According to a side-by-side self-assembling model proposed previously,[26] this different width might be determined by different

https://doi.org/10.1021/acsomega.1c01423
ACS Omega 2021, 6, 12904−12912

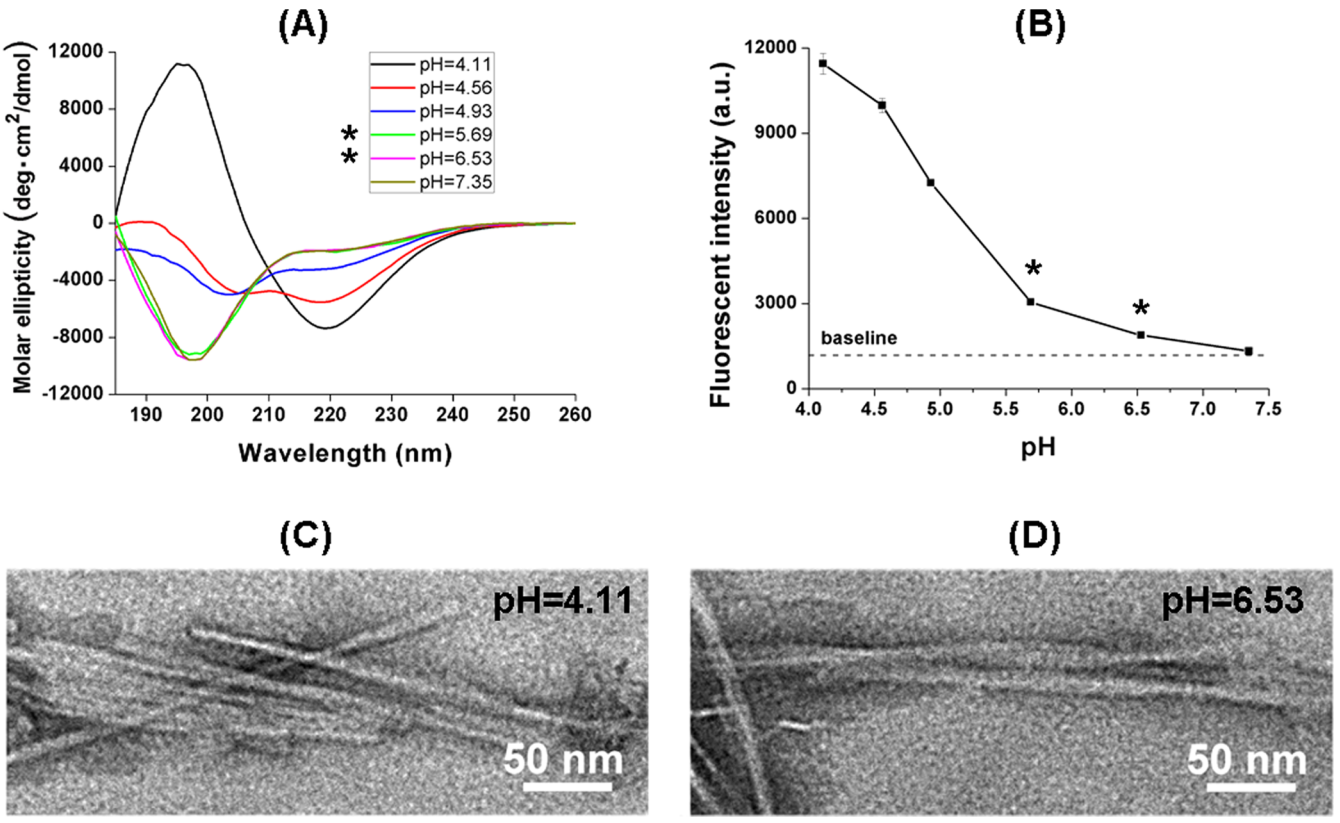

Figure 4. pH-induced conformational transition and disassembly of RADA16-I. (A) CD spectra showed the conformational transition from β-strand to the disordered secondary structure, with the total loss of β-strand at pH 5.69 and 6.53 (marked by stars). (B) ThT-binding fluorescence showed the disassembling process, with nanofibers retained at pH 5.69 and 6.53 (marked by stars). (C) TEM image of nanofibers formed at pH 4.11. (D) TEM image of nanofibers formed at pH 6.53.

secondary structures the peptide was taking at different concentrations. As shown in Figure 2E, peptide backbones in disordered conformation could be freely extended and assemble into wider nanofibers, while at higher concentrations, the peptide transformed into β-strand, which could be compactly packed and form narrower nanofibers.

Similar to RADA16-I, an amphiphilic peptide DA6D also exhibited obvious fibrillization behavior at low concentrations when the peptide was still in disordered conformation. As shown in Figure S4A, DA6D was kept in an unchanged disordered conformation at concentrations of 50, 100, and 200 μM, and the typical β-strand signal began to occur above 400 μM. However, the peptide began to show the obvious fibrillization signal from 100 μM and above, as shown in Figure S4B, suggesting that disordered conformation could also support the fibrillization process of DA6D. Furthermore, TEM images in Figure S4C showed that at lower concentrations, disordered conformation led to the formation of helical ribbons, while at higher concentrations, β-strand led to the formation of smooth nanofibers, exhibiting a more compact manner of assembly (Figure S4D).

Hydrophobic Interaction for RADA16-I Fibrillization. Such concentration-dependent self-assembling behavior generally indicated the involvement of hydrophobic interaction as a major driving force for self-assembly, which has also been repeatedly mentioned by previous studies. As shown in Figure 3A, in the pyrene-binding fluorescence spectrum of RADA16-I, the third peak (I3) was obviously higher than that of pyrene in H_2O, indicating the existence of hydrophobic interaction in RADA16-I nanofibers. As shown in Figure 3B, 8-anilinonaphthalene-1-sulfonic acid (ANS)-binding fluorescence of RADA16-I exhibited an obvious blue shift and enhancement compared with the ANS spectrum in H_2O, which was also a feature of hydrophobic interaction. It is likely that the self-assembly of RADA16-I relied more on hydrophobic interaction determined by peptide concentration, while the secondary structure of the peptide monomer was not so determinative. Even in disordered conformation, a peptide chain could still be freely extended, exposing its hydrophobic residues for coupling with other peptides through hydrophobic interaction. This may also explain why we observed the self-assembling nanofibers with the absence of the β-sheet.

To further prove that a hydrophobic interaction played a predominant role in the self-assembly of RADA16-I, the self-assembling behavior of RADA16-I with the presence of organic solvents was investigated. As shown in Figure 3, although 100 μM RADA16-I formed more typical β-strand as induced by ethanol or *n*-propanol (Figure 3C), its self-assembling ability drastically decreased by the presence of organic solvents in a concentration-dependent manner (Figure 3D). A possible reason is that ethanol and *n*-propanol have lower polarity than water; therefore, they could weaken water-mediated hydrophobic interaction and decrease the peptide's aggregation potency based on it. It is also clear that *n*-propanol with even lower polarity showed an even greater impact on the self-assembling ability. These results further indicated that for the fibrillization of RADA16-I, hydrophobic interaction as a major driving force was more important than β-strand conformation, especially considering that the peptide in a more typical β-

https://doi.org/10.1021/acsomega.1c01423
ACS Omega 2021, 6, 12904−12912

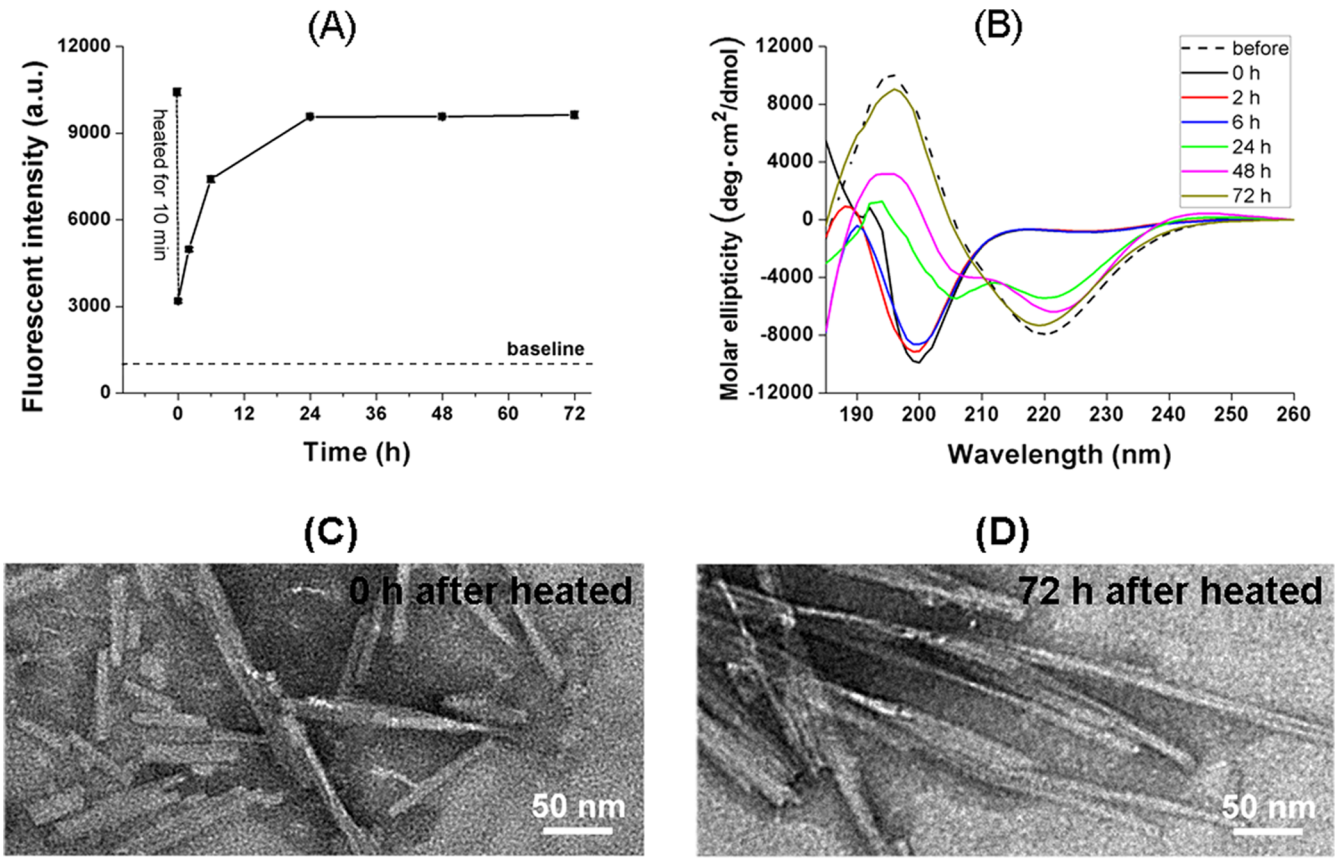

Figure 5. Heat recovery process of RADA16-I. (A) Time-dependent change in the ThT-binding fluorescence of RADA16-I after heating. (B) Time-dependent change in the CD spectra of RADA16-I after heating. (C) TEM image of nanofibers formed by RADA16-I immediately after heating. (D) TEM image of nanofibers formed by RADA16-I 72 h after heating.

strand conformation showed even lower fibrillization signal in this experiment.

pH-Responsive Fibrillization of RADA16-I. Except for relying on hydrophobic interaction, fibrillization of RADA16-I was also known to be supported by electrostatic interaction between positively charged arginine and negatively charged aspartic acid residues. Since the charge distribution of the two amino acids was determined by the pH of the peptide solution, fibrillization of RADA16-I was also a pH-responsive process.

Although the disassembly of RADA16-I nanofibers in response to pH increase was nothing new, it has been presumed that pH increase led to the conformational transition from β-strand to disordered conformation, which further led to the disassembly of nanofibers. This means that the loss of β-strand was the direct cause of disassembly. However, an alternative pathway for this pH-responsive change was found in our study by monitoring the change in the secondary structure and the fibrillization state of 200 μM RADA16-I at different pH values. As shown in Figure 4A, with the pH increasing from 4.11 to 7.35, the peptide gradually transformed from β-strand to disordered conformation, with the total loss of the β-strand signal at pH 5.69 and above. On the other hand, Figure 4B shows that the self-assembling ability of RADA16-I also decreased with the increase of pH, but the peptide still showed the fibrillization signal at pH 5.69 and 6.53, when it was already in a stable disordered conformation. When the peptide took disordered conformation at pH 6.53, it formed helical nanofibers wider than those formed at pH 4.11 when it was in β-strand conformation (Figure 4C,D). Additional TEM images of nanofibers formed at pH 4.11 or 6.53 are shown in Figure S5. Furthermore, as shown in Figure S6, the sample with pH 4.11 exhibited a broad size distribution between 30 and 2000 nm, while the size distribution of the sample with pH 6.53 was around 100 nm. Combined with the TEM and ThT-binding fluorescence data, these results suggested that RADA16-I formed more and longer nanofibers at pH 4.11, while its fibrillization was weakened at pH 6.53.

These results indicated that in the pH-induced disassembling process of RADA16-I nanofibers, even when the β-sheet completely disappeared, the peptide could still form nanofibers based on disordered conformation. In a reverse logic, it could also be concluded that with the decrease of pH from 7.35 to 4.11, RADA16-I gradually underwent fibrillization starting from disordered conformation, and in some middle point of the fibrillization process, the peptide began to transform from disordered conformation to β-strand.

Time-Dependent Reassembling Process after the Heat Shock. Because of the existence of amide groups along the peptide backbone, the self-assembly of RADA16-I also involved intermolecular hydrogen bond, which could be temporarily destroyed at a high temperature and recover upon incubation at a lower temperature. This provided us a starting point to monitor the dynamic conformational transition and fibrillization during the heat recovery process in a time-dependent manner. As shown in Figure 5A, after incubation at 70 °C for 10 min, ThT-binding fluorescence of RADA16-I dropped sharply, but the fluorescence value was still far above the baseline, indicating an incomplete disassembly of nano-

https://doi.org/10.1021/acsomega.1c01423
ACS Omega 2021, 6, 12904−12912

fibers upon heating. Then, during incubation at 25 °C, the peptide gradually reassembled and the ThT-binding fluorescence reached a plateau after 24 h. On the other hand, as shown in Figure 5B, the secondary structure of the peptide completely transformed from β-strand to disordered conformation after the heat shock, indicating that β-strand was more vulnerable than the self-assembling structures upon heating. During the first 6 h of recovery, the peptide only slightly lost its signal of disordered conformation around 200 nm despite the rapid growth of ThT-binding fluorescence at the same time. After 24 h, the peptide began to show the β-strand signal around 220 nm, which gradually transformed to typical β-strand after 72 h, even though the peptide had already been in its mature fibrillization state after 24 h. TEM images showed that after heating, RADA16-I formed shorter and wider nanofibers (Figure 5C), which could reassemble into longer and narrower nanofibers after 72 h (Figure 5D). Additional TEM images of nanofibers formed at 0 or 72 h after heating are shown in Figure S7. Furthermore, as shown in Figure S8, the size distribution of RADA16-I immediately after heating was around 100 nm, which changed to a broader distribution between 20 and 700 nm at 72 h after heating. Combined with the TEM and ThT-binding fluorescence data, these results further indicated the recovery of long nanofibers after heating.

On one hand, the results of the heat recovery experiments showed again that RADA16-I could retain its self-assembling nanofibers based on disordered conformation. On the other hand, it is interesting that during the reassembling process, RADA16-I reached its maximum fibrillization state first, following which its secondary structure slowly transformed from disordered conformation to β-strand. On the contrary to the traditional belief that β-sheets induce the fibrillization of RADA16-I, it seemed that fibrillization could take place first, which then induced the formation of the β-sheet, probably by physically pressing the peptides in compact nanofibers and forced them to take a more ordered β-strand conformation.

CONCLUSIONS

Based on the truth that the β-sheet is the predominant structure in mature RADA16-I nanofibers, it has been generally believed that β-strand is the structural basis for fibrillization of the peptide. This theory has also been used to explain how a peptide changes its fibrillization state in response to environmental parameters such as pH and temperature in a β-strand-first way. However, in this study, we reported an unexpected fibrillization pathway of RADA16-I in a low concentration range. By studying the causal link between the fibrillization process and the formation of β-strand under different concentrations and environmental conditions, we found that early-stage fibrillization of RADA16-I could happen based on the disordered secondary structure, and then a β-sheet could be formed later than that. Even though RADA16-I was in disordered conformation, noncovalent forces such as hydrophobic interaction and electrostatic interaction could drive the fibrillization behavior, and during this fibrillization process, the peptide could be pressed into an ordered β-sheet. Except for our experimental findings reported in this work, some earlier computational studies have also suggested that β-strand conformation could rise as a result of water-mediated peptide folding.[33,34] These results reevaluated the importance of typical β-strand for peptide fibrillization, providing a deeper insight into the general mechanism of peptide self-assembly. More detailed information in the disordered secondary structure could be further exploited, for example, by analyzing the peptide sequence in detail.[35,36] This would be important for further clarifying how such disordered peptide monomers support fibrillization.

According to our new findings, when designing SAP nanofiber materials based on RADA16-I or other self-assembling motifs, the intrinsic β-strand secondary structure should not be overconcerned. Instead, we should focus on parameters such as overall hydrophobicity and charge distribution, which directly provide the driving force for the fibrillization process. On the other hand, since this study was focused on the initial stage of peptide fibrillization at a very low concentration, our findings also provided important clues for studying amyloid-like aggregation processes of natural peptides or proteins, which always gradually accumulated from a very low concentration. According to our findings on RADA16-I, more attention should be focused on parameters directly driving the aggregation rather than β-strand conformation.

METHODS

Peptides and Reagents. Peptides Ac-RADARADARA-DARADA-NH_2 (RADA16-I) and DAAAAAAD (DA6D) were purchased from Shanghai Bootech Bioscience & Technology Co., Ltd. (Shanghai, China) as lyophilized powders with purity over 95%. Thioflavin-T (ThT), pyrene, and 8-anilinonaphthalene-1-sulfonic acid (ANS) were purchased from Sigma-Aldrich Co. (St. Louis, MO). Ethanol and *n*-propanol were purchased from Chengdu Chron Chemicals Co., Ltd. (Chengdu, China). Peptide solutions with different concentrations were prepared by dissolving peptide powders in Milli-Q water or its mixture with ethanol or *n*-propanol as specified in the corresponding sections. The original pH of the RADA16-I water solution with a concentration of 200 μM was 4.11, which was adjusted to different pH values using 0.1 M NaOH. All samples were incubated at room temperature (RT) for at least 7 days before the experiment.

CD Spectra Measurement. A Model 400 CD spectrophotometer (Aviv Biomedical Inc.,) was used to collect CD signals of peptide samples filled in a quartz cuvette with a path length of 0.2 cm. For each sample, CD spectra between 185 and 260 nm were measured three times to get an averaged spectrum, which was then converted to molar ellipticity (ME) using the following equation

$$\mathrm{ME} = \frac{\mathrm{CDs}}{n \times c \times l \times 10}$$

where CDs is the CD signal collected for each sample, n is the number of amino acid residues in RADA16-I (i.e., 16), c is the molar concentration of each sample, and l is the path length of the cuvette (i.e., 0.2 cm).

ThT-Binding Test. The ThT powder was dissolved in Milli-Q water as a 1 mM stock solution. For the ThT-binding test, 500 μL of the peptide sample was mixed with 5 μL of the ThT stock solution, and a Fluorolog spectrometer (Horiba Scientific Inc.) was used to collect the fluorescence spectrum between 460 and 600 nm with an excitation wavelength of 450 nm. Each sample was measured three times to get an averaged peak value at 495 nm. Milli-Q water mixed with ThT at the same ratio was measured to obtain a baseline value at 495 nm.

Size Distribution Analysis by DLS. The size distribution of nanostructures formed in different peptide solutions was measured by DLS using a Zetasizer Nano-ZS instrument

https://doi.org/10.1021/acsomega.1c01423
ACS Omega 2021, 6, 12904−12912

(Malvern, U.K.). Briefly, 1.5 mL of each peptide solution was added into a disposable sizing cuvette and kept at 25 °C for 30 s prior to measurement. Intensity data were collected and size versus fraction distribution plots were obtained. Each measurement showed the averaged result of 20 rounds of collection, and for each sample, five independent measurements were performed to ensure that similar results were obtained.

TEM Observation. To observe the morphology of nanofibers formed by RADA16-I and DA6D, 20 μL of each peptide solution was kept on a copper grid covered by Formvar and carbon films for 3−10 min, after which excess solution was blotted away with a filter paper. Then, 20 μL of 2% phosphotungstic acid was dropped onto the grid to stain the sample for 2−3 min, and excess liquid was carefully blotted away with a filter paper without leaving any visible liquid on the grid. The grid was then completely air-dried and observed with TEM (Tecnai G2 F20, FEI). For each sample, 3−5 different areas on the grid were observed to ensure the prevalence of similar nanostructures.

Pyrene-Binding Fluorescence. A pyrene stock solution with a concentration of 2 mM was prepared in dimethyl sulfoxide. An RADA16-I solution with a concentration of 100 μM was mixed with the pyrene stock solution at a volume ratio of 500:1 and incubated at RT for 10 min. The pyrene stock solution diluted in H_2O at the same ratio was used as control. Fluorescence spectra between 360 and 440 nm were collected using a Fluorolog spectrometer with an excitation wavelength of 336 nm. The first peak (I1) of the two spectra was normalized to compare the intensity of the third peak (I3).

ANS-Binding Fluorescence. An ANS stock solution with a concentration of 2 mM was prepared in sodium phosphate buffer (pH 7.4). For the ANS-binding test, the RADA16-I solution with a concentration of 100 μM was mixed with the ANS stock solution at a volume ratio of 100:1 and incubated at RT for 10 min. The ANS stock solution diluted in H_2O at the same ratio was used as control. Fluorescence spectra between 400 and 600 nm were collected using a Fluorolog spectrometer with an excitation wavelength of 350 nm.

Heat Shock Experiment. A water solution of RADA16-I with a concentration of 200 μM was prepared as previously described. The sample was heated at 70 °C in a metal bath for 10 min and aliquoted for continuous CD spectra and ThT-binding fluorescence measurement at desired intervals of 0, 2, 6, 24, 48, and 72 h. The aliquots of the samples on 0 and 72 h were also used for TEM observation as previously described.

■ ASSOCIATED CONTENT

Supporting Information

The Supporting Information is available free of charge at https://pubs.acs.org/doi/10.1021/acsomega.1c01423.

ThT-binding fluorescent spectrum; additional TEM images; DLS data; CD, ThT-binding fluorescence; and TEM data of the DAD peptide (PDF)

■ AUTHOR INFORMATION

Corresponding Author

Feng Qiu − *Laboratory of Anesthesia and Critical Care Medicine, Translational Neuroscience Center and National Clinical Research Center for Geriatrics, West China Hospital, Sichuan University, Chengdu 610041, China; National-Local Joint Engineering Research Center of Translational Medicine of Anesthesiology, West China Hospital, Sichuan University, Chengdu 610041, China;* orcid.org/0000-0002-0450-229X; Email: fengqiu@scu.edu.cn

Authors

Zhihua Xing − *Laboratory of Anesthesia and Critical Care Medicine, Translational Neuroscience Center and National Clinical Research Center for Geriatrics, West China Hospital, Sichuan University, Chengdu 610041, China; Laboratory of Ethnopharmacology, West China Hospital, Sichuan University, Chengdu 610041, China*

Yongzhu Chen − *Laboratory of Anesthesia and Critical Care Medicine, Translational Neuroscience Center and National Clinical Research Center for Geriatrics, West China Hospital, Sichuan University, Chengdu 610041, China; Periodical Press of West China Hospital, Sichuan University, Chengdu 610041, China*

Complete contact information is available at: https://pubs.acs.org/10.1021/acsomega.1c01423

Notes

The authors declare no competing financial interest.

■ ACKNOWLEDGMENTS

This work was financially supported by the National Clinical Research Center for Geriatrics, West China Hospital, Sichuan University (Z2018B21) and the National Natural Science Foundation of China (Nos. 81000658 and 31100565).

■ REFERENCES

(1) Zhang, S. Discovery and design of self-assembling peptides. *Interface Focus* **2017**, *7*, No. 20170028.

(2) Yang, Z.; Xu, H.; Zhao, X. Designer self-assembling peptide hydrogels to engineer 3D cell microenvironments for cell constructs formation and precise oncology remodeling in ovarian cancer. *Adv. Sci.* **2020**, *7*, No. 1903718.

(3) Koutsopoulos, S. Self-assembling peptide nanofiber hydrogels in tissue engineering and regenerative medicine: Progress, design guidelines, and applications. *J. Biomed. Mater. Res., Part A* **2016**, *104*, 1002−1016.

(4) Chen, Y.; Xing, Z.; Liao, D.; Qiu, F. Neglected hydrophobicity of dimethanediyl group in peptide self-assembly: A hint from amyloid-like peptide GNNQQNY and its derivatives. *J. Phys. Chem. B* **2018**, *122*, 10470−10477.

(5) Ke, P. C.; Sani, M. A.; Ding, F.; Kakinen, A.; Javed, I.; Separovic, F.; Davis, T. P.; Mezzenga, R. Implications of peptide assemblies in amyloid diseases. *Chem. Soc. Rev.* **2017**, *46*, 6492−6531.

(6) Tan, J.; Zhang, J.; Luo, Y.; Ye, S. Misfolding of a human islet amyloid polypeptide at the lipid membrane populates through β-sheet conformers without involving α-helical intermediates. *J. Am. Chem. Soc.* **2019**, *141*, 1941−1948.

(7) Gelenter, M. D.; Smith, K. J.; Liao, S. Y.; Mandala, V. S.; Dregni, A. J.; Lamm, M. S.; Tian, Y.; Xu, W.; Pochan, D. J.; Tucker, T. J.; Su, Y.; Hong, M. The peptide hormone glucagon forms amyloid fibrils with two coexisting β-strand conformations. *Nat. Struct. Mol. Biol.* **2019**, *26*, 592−598.

(8) Sun, Y.; Kakinen, A.; Xing, Y.; Faridi, P.; Nandakumar, A.; Purcell, A. W.; Davis, T. P.; Ke, P. C.; Ding, F. Amyloid self-assembly of hIAPP8-20 via the accumulation of helical oligomers, α-helix to β-sheet transition, and formation of β-barrel intermediates. *Small* **2019**, *15*, No. e1805166.

(9) Sivanesam, K.; Andersen, N. Pre-structured hydrophobic peptide β-strands: A universal amyloid trap? *Arch. Biochem. Biophys.* **2019**, *664*, 51−61.

(10) Kim, S.; Kim, J. H.; Lee, J. S.; Park, C. B. Beta-sheet-forming, self-assembled peptide nanomaterials towards optical, energy, and healthcare applications. *Small* **2015**, *11*, 3623−3640.

(11) Cui, H.; Webber, M. J.; Stupp, S. I. Self-assembly of peptide amphiphiles: from molecules to nanostructures to biomaterials. *Biopolymers* **2010**, *94*, 1−18.
(12) Ilawe, N. V.; Schweitzer-Stenner, R.; DiGuiseppi, D.; Wong, B. M. Is a cross-β-sheet Structure of low molecular weight peptides necessary for the formation of fibrils and peptide hydrogels? *Phys. Chem. Chem. Phys.* **2018**, *20*, 18158−18168.
(13) Milorey, B.; Farrell, S.; Toal, S. E.; Schweitzer-Stenner, R. Demixing of water and ethanol causes conformational redistribution and gelation of the cationic GAG tripeptide. *Chem. Commun.* **2015**, *51*, 16498−16501.
(14) Shang, Y.; Wang, Z.; Zhang, R.; Li, X.; Zhang, S.; Gao, J.; Li, X.; Yang, Z. A novel thermogel system of self-assembling peptides manipulated by enzymatic dephosphorylation. *Chem. Commun.* **2019**, *55*, 5123−5126.
(15) Vilaça, H.; Castro, T.; Costa, F. M. G.; Melle-Franco, M.; Hilliou, L.; Hamley, I. W.; Castanheira, E. M. S.; Martins, J. A.; Ferreira, P. M. T. Self-assembled RGD dehydropeptide hydrogels for drug delivery applications. *J. Mater. Chem. B* **2017**, *5*, 8607−8617.
(16) Qiu, F.; Chen, Y.; Tang, C.; Zhou, Q.; Wang, C.; Shi, Y.-K.; Zhao, X. De novo design of a bolaamphiphilic peptide with only natural amino acids. *Macromol. Biosci.* **2008**, *8*, 1053−1059.
(17) Qiu, F.; Chen, Y.; Zhao, X. Comparative studies on the self-assembling behaviors of cationic and catanionic surfactant-like peptides. *J. Colloid Interface Sci.* **2009**, *336*, 477−484.
(18) Qiu, F.; Tang, C.; Chen, Y. Amyloid-like aggregation of designer bolaamphiphilic peptides: Effect of hydrophobic section and hydrophilic heads. *J. Pept. Sci.* **2018**, *24*, No. e3062.
(19) Lee, O.-S.; Stupp, S. I.; Schatz, G. C. Atomistic molecular dynamics simulations of peptide amphiphile self-assembly into cylindrical nanofibers. *J. Am. Chem. Soc.* **2011**, *133*, 3677−3683.
(20) Deshmukh, S. A.; Solomon, L. A.; Kamath, G.; Fry, H. C.; Sankaranarayanan, S. K. R. S. Water ordering controls the dynamic equilibrium of micelle-fibre formation in self-assembly of peptide amphiphiles. *Nat. Commun.* **2016**, *7*, No. 12367.
(21) Argudo, P. G.; Giner-Casares, J. J. Folding and self-assembly of short intrinsically disordered peptides and protein regions. *Nanoscale Adv.* **2021**, *3*, 1789−1812.
(22) Hoffmann, W.; Folmert, K.; Moschner, J.; Huang, X.; von Berlepsch, H.; Koksch, B.; Bowers, M. T.; von Helden, G.; Pagel, K. The onset of beta-sheet formation and the mechanism for fibril formation. *J. Am. Chem. Soc.* **2018**, *140*, 244−249.
(23) Gong, Z.; Liu, X.; Dong, J.; Zhang, W.; Jiang, Y.; Zhang, J.; Feng, W.; Chen, K.; Bai, J. Transition from vesicles to nanofibres in the enzymatic self-assemblies of an amphiphilic peptide as an antitumour drug carrier. *Nanoscale* **2019**, *11*, 15479−15486.
(24) Cheng, B.; Yan, Y.; Qi, J.; Deng, L.; Shao, Z. W.; Zhang, K. Q.; Li, B.; Sun, Z.; Li, X. Cooperative assembly of a peptide gelator and silk fibroin afford an injectable hydrogel for tissue engineering. *ACS Appl. Mater. Interfaces* **2018**, *10*, 12474−12484.
(25) Zhang, C.; Shafi, R.; Lampel, A.; MacPherson, D.; Pappas, C. G.; Narang, V.; Wang, T.; Maldarelli, C.; Ulijn, R. V. Switchable hydrolase based on reversible formation of supramolecular catalytic site using a self-assembling peptide. *Angew. Chem., Int. Ed.* **2017**, *56*, 14511−14515.
(26) Yokoi, H.; Kinoshita, T.; Zhang, S. Dynamic reassembly of peptide RADA16 nanofiber scaffold. *Proc. Natl. Acad. Sci. U.S.A.* **2005**, *102*, 8414−8419.
(27) Cormier, A. R.; Pang, X.; Zimmerman, M. I.; Zhou, H. X.; Paravastu, A. K. Molecular structure of RADA16-I designer self-assembling peptide nanofibers. *ACS Nano* **2013**, *7*, 7562−7572.
(28) Bagrov, D.; Gazizova, Y.; Podgorsky, V.; Udovichenko, I.; Danilkovich, A.; Prusakov, K.; Klinov, D. Morphology and aggregation of RADA-16-I peptide Studied by AFM, NMR and molecular dynamics simulations. *Biopolymers* **2016**, *106*, 72−81.
(29) Zhao, Y.; Zhu, R.; Song, X.; Ma, Z.; Chen, S.; Wu, D.; Liu, F.; Ouyang, S.; Zhang, J.; Ramakrishna, S.; Zhu, X.; He, L. Assembly pathway selection of designer self-assembling peptide and fabrication of hierarchical scaffolds for neural regeneration. *ACS Appl. Mater. Interfaces* **2018**, *10*, 26128−26141.
(30) Wu, D.; Zhang, S.; Zhao, Y.; Ao, N.; Ramakrishna, S.; He, L. The effects of motif net charge and amphiphilicity on the self-assembly of functionally designer RADA16-I peptides. *Biomed. Mater.* **2018**, *13*, No. 035011.
(31) Castelletto, V.; Hamley, I. W. Methods to characterize the nanostructure and molecular organization of amphiphilic peptide assemblies. *Methods Mol. Biol.* **2018**, *1777*, 3−21.
(32) Chen, Y.; Hua, Y.; Zhang, W.; Tang, C.; Wang, Y.; Zhang, Y.; Qiu, F. Amyloid-like staining property of RADA16-I nanofibers and its potential application in detecting and imaging the nanomaterial. *Int. J. Nanomed.* **2018**, *13*, 2477−2489.
(33) Kumar, A.; Schweitzer-Stenner, R.; Wong, B. M. A new interpretation of the structure and solvent dependence of the far UV circular dichroism spectrum of short oligopeptides. *Chem. Commun.* **2019**, *55*, 5701−5704.
(34) Ilawe, N. V.; Raeber, A. E.; Schweitzer-Stenner, R.; Toal, S. E.; Wong, B. M. Assessing backbone solvation effects in the conformational propensities of amino acid residues in unfolded peptides. *Phys. Chem. Chem. Phys.* **2015**, *17*, 24917−24924.
(35) Toal, S. E.; Kubatova, N.; Richter, C.; Linhard, V.; Schwalbe, H.; Schweitzer-Stenner, R. Randomizing the unfolded state of peptides (and proteins) by nearest neighbor interactions between unlike residues. *Chem. - Eur. J.* **2015**, *21*, 5173−5192.
(36) Milorey, B.; Schweitzer-Stenner, R.; Andrews, B.; Schwalbe, H.; Urbanc, B. Short peptides as predictors for the structure of polyarginine sequences in disordered proteins. *Biophys. J.* **2021**, *120*, 662−676.

https://doi.org/10.1021/acsomega.1c01423
ACS Omega 2021, 6, 12904−12912